Neurobiology of Disease 182 (2023) 106146

Contents lists available at ScienceDirect

Neurobiology of Disease

journal homepage: www.elsevier.com/locate/ynbdi

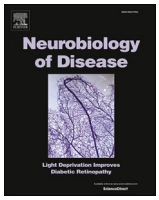

Early-onset brain alterations during postnatal development in a mouse model of CDKL5 deficiency disorder

Marianna Tassinari [1], Beatrice Uguagliati [1], Stefania Trazzi, Camilla Bruna Cerchier, Ottavia Vera Cavina, Nicola Mottolese, Manuela Loi, Giulia Candini, Giorgio Medici, Elisabetta Ciani [*]

Department of Biomedical and Neuromotor Science, University of Bologna, 40126 Bologna, Italy

ARTICLE INFO

Keywords:
Cdkl5 KO mice
Brain development
Dendritic pathology
Neuronal survival
Neuroinflammation

ABSTRACT

Mutations in the *CDKL5* gene are the cause of CDKL5 deficiency disorder (CDD), a rare and severe neurodevelopmental condition characterized by early-onset epilepsy, motor impairment, intellectual disability, and autistic features. A mouse model of CDD, the *Cdkl5* KO mouse, that recapitulates several aspects of CDD symptomology, has helped to highlight brain alterations leading to CDD neurological defects. Studies of brain morphogenesis in adult *Cdkl5* KO mice showed defects in dendritic arborization of pyramidal neurons and in synaptic connectivity, a hypocellularity of the hippocampal dentate gyrus, and a generalized microglia overactivation. Nevertheless, no studies are available regarding the presence of these brain alterations in *Cdkl5* KO pups, and their severity in early stages of life compared to adulthood. A deeper understanding of the CDKL5 deficient brain during an early phase of postnatal development would represent an important milestone for further validation of the CDD mouse model, and for the identification of the optimum time window for treatments that target defects in brain development. In sight of this, we comparatively evaluated the dendritic arborization and spines of cortical pyramidal neurons, cortical excitatory and inhibitory connectivity, microglia activation, and proliferation and survival of granule cells of the hippocampal dentate gyrus in hemizygous *Cdkl5* KO male (−/Y) mice aged 7, 14, 21, and 60 days. We found that most of the structural alterations in *Cdkl5* −/Y brains are already present in pups aged 7 days and do not worsen with age. In contrast, the difference in the density of excitatory and inhibitory terminals between *Cdkl5* −/Y and wild-type mice changes with age, suggesting an age-dependent cortical excitatory/inhibitory synaptic imbalance. Confirming the precocious presence of brain defects, *Cdkl5* −/Y pups are characterized by an impairment in neonatal sensory-motor reflexes.

1. Introduction

Loss-of-function variants in the X-linked cyclin-dependent kinase like 5 (*CDKL5*) gene (MIM 300203) underpin a severe developmental encephalopathy named CDKL5 Deficiency Disorder (CDD; OMIM 300203, 300672). This rare genetic neurodevelopmental disorder has a worldwide incidence of approximately 1: 40,000–60,000 live births (Symonds et al., 2019), with higher frequency in females than in males (~4:1; (Lopez-Rivera et al., 2020)). The clinical manifestation of CDD usually begin during early infancy, with variable and complex combinations of symptoms including early-onset drug-resistant seizures (in the first days/months of life), and a severe neurodevelopmental impairment with major motor development delay such as generalized hypotonia and retardation of psychomotor development (already observed in the first few months of life). Cortical visual impairment, severe intellectual disability, and gastrointestinal and orthopaedic complaints are common (Bahi-Buisson and Bienvenu, 2012; Jakimiec et al., 2020; Olson et al., 2019). Currently, no cure is available for CDD patients; pharmacological treatments mostly address seizure management, and no effective treatments exist to ameliorate the cognitive and behavioral symptoms of

Abbreviations: CDKL5, cyclin-dependent kinase-like 5; CDD, CDKL5 deficiency disorder; VGluT1, vesicular glutamate transporter 1; GABA, gamma-aminobutyric acid; VGAT, vesicular GABA transporter; AIF1, anti-allograft inflammatory factor 1; DCX, doublecortin; DG, dentate gyrus; GL, granular layer; SGZ, subgranular zone; EB2, microtubule end-binding protein 2; CNS, central nervous system.

* Corresponding author at: Department of Biomedical and Neuromotor Sciences, Piazza di Porta San Donato 2, 40126 Bologna, Italy.
E-mail addresses: stefania.trazzi3@unibo.it (S. Trazzi), elisabetta.ciani@unibo.it (E. Ciani).
[1] These authors contributed equally to this work.

https://doi.org/10.1016/j.nbd.2023.106146
Received 9 March 2023; Received in revised form 5 May 2023; Accepted 7 May 2023
Available online 8 May 2023

CDD.

Studies in rodents have shown that Cdkl5 is expressed at low levels during embryonic stages, and that its expression rapidly increases postnatally in neurons. The peak of Cdkl5 expression during the postnatal period suggests that CDKL5 functions are required early on to ensure proper brain formation/function (Rusconi et al., 2008; Zhu et al., 2013). Several knockout (KO) mouse models for *Cdkl5* have been developed to address how CDKL5 dysfunction leads to neurological defects in CDD (Amendola et al., 2014; Okuda et al., 2017; Wang et al., 2012). To date, studies on *Cdkl5* KO mice have focused mainly on the adult brain phenotype. In particular, *Cdkl*5 KO mouse models exhibit several behavioral phenotypes that mimic CDD features, such as impaired learning and memory, social interaction, and motor coordination, together with increased stereotypy (Amendola et al., 2014; Fuchs et al., 2015; Fuchs et al., 2014; Ren et al., 2019; Wang et al., 2012). These defects are associated with neuroanatomical alterations: reduced neuronal branching, spine maturation, and connectivity observed in the cortex and in the hippocampal region of *Cdkl5* KO mice (Amendola et al., 2014; Fuchs et al., 2015; Fuchs et al., 2014; Gennaccaro et al., 2021; Pizzo et al., 2016, Della Sala et al., 2016; Ren et al., 2019). In addition, *Cdkl5* KO mice are characterized by an increased rate of apoptotic cell death in the hippocampal dentate gyrus and by an increased status of microglia overactivation, indicating that an absence of Cdkl5 increases neuronal vulnerability (Fuchs et al., 2014; Galvani et al., 2021; Gennaccaro et al., 2021; Loi et al., 2020). These studies present considerable evidence that a number of brain developmental deficits can be identified and that these deficits underlie the well-characterized phenotype in juvenile and adult *Cdkl5* KO mice. Nevertheless, no studies are available regarding the presence of these brain alterations in *Cdkl5* KO pups and unclear or untested issues remain regarding the development of symptomology and underlying mechanisms. This knowledge is of obvious importance for the identification of an optimum time window for treatments that target defects during brain development and for further validation of the mouse model, through the description of the altered crucial stages of early brain maturation in CDD.

Based on these premises, the goal of the current study was to establish whether defects in brain development, including dendritic complexity and spine maturation, excitatory and inhibitory connectivity, microglia activation, and neuronal survival, are already present in the brain of *Cdkl5* KO pups, or, if not, to determine at what stage they appear and evolve during postnatal brain development. Since spine density reduction is a typical feature of the dendritic pathology that affects the brain of adult *Cdkl5* −/Y mice, we conducted our analyses starting from 7-day-old *Cdkl5* −/Y mice because dendric spines are generated approximately at the end of the first postnatal week in rodents (Eller et al., 1969; Juraska and Fifkova, 1979; Yuste and Bonhoeffer, 2004). As structural defects are reflected in altered behavior, *Cdkl5* −/Y pups were tested for motor-reflex behavior responses, as an indication of impaired neurological development.

2. Materials and methods

2.1. Colony

The mice used in this work derived from the *Cdkl5* KO strain in the C57BL/6N background developed in (Amendola et al., 2014) and backcrossed in C57BL/6J for three generations. Age-matched wild-type (+/Y) littermate controls were used for all experiments. The day of birth was designated as postnatal day zero (P0) and animals with 24 h of age were considered as 1-day-old animals (P1). Mice for experiments were produced by crossing *Cdkl*5 +/− heterozygous females with wild-type (+/Y) males and were karyotyped by PCR on genomic DNA as previously described (Amendola et al., 2014). Mice were housed three to five per cage and maintained in a temperature- (23 °C) and humidity-controlled environment with a standard 12 h light/dark cycle, and were provided with standard mouse chow and water ad libitum. The animals' day-to-day health and comfort were controlled by the veterinary service. Experiments were performed in accordance with the Italian and European Community law for the use of experimental animals and were approved by Bologna University Bioethical Committee. In this study, all efforts were made to minimize animal suffering and to keep the number of animals used to a minimum. The number of animals used for each experimental procedure is specified in the figure legends.

2.2. Histological and immunohistochemistry procedures

Cdkl5 -/Y mice and +/Y littermates were anesthetized with 2% isoflurane (in pure oxygen) and sacrificed at postnatal day 7 (P7), 14 (P14), 21 (P21), and 60 (P60). Body weight was recorded prior to sacrifice. Brains were quickly removed and cut along the midline. Right hemispheres were Golgi-stained or quickly frozen and used for Western blot analyses (see description below). Left hemispheres were fixed via immersion in 4% paraformaldehyde (100 mM phosphate buffer, pH 7.4) for 48 h, kept in 15–20% sucrose for an additional 24 h, and then frozen with cold ice. Hemispheres were cut with a freezing microtome into 30-μm-thick coronal sections and processed for immunohistochemistry procedures as described below. One out of 6 sections from the hippocampal formation and somatosensory cortex were used for immunohistochemistry for vesicular glutamate transporter 1 (VGluT1), vesicular GABA transporter (VGAT), anti-allograft inflammatory factor 1 (AIF1), Ki67 or doublecortin (DCX) following the protocol published in (Fuchs et al., 2014; Galvani et al., 2021; Pizzo et al., 2016). Nuclei were counterstained with Hoechst 33342 (Sigma-Aldrich). The primary and secondary antibodies used are listed in Supplementary Table 1.

2.3. Golgi staining

Hemispheres were Golgi-stained using the FD Rapid Golgi Stain TM Kit (FD NeuroTechnologies, Inc.) as previously described (Guidi et al., 2013). The hemispheres were cut with a cryostat into 100 μm-thick coronal sections. Sections were mounted directly onto super frost slides and air dried at room temperature. After drying, sections were rinsed with distilled water, stained in the developing solution of the kit and coverslipped with DPX mounting medium.

2.4. Image acquisition and measurements

Fluorescence images were taken with an Eclipse TE 2000-S microscope equipped with a DS-Qi2 digital SLR camera (Nikon Instruments Inc.). A light microscope (Leica Mycrosystems) equipped with a motorized stage and focus control system and a color digital camera (Coolsnap-Pro, Media Cybernetics) were used for neuronal tracing and to take bright field images. Measurements were carried out using the Image Pro Plus software (Media Cybernetics, Silver Spring, MD, USA), by investigators blind to the animal's genotype.

2.4.1. Measurement of the dendritic tree

Dendritic trees were traced using custom-designed software for dendritic reconstruction (Immagini Computer, Milan, Italy), interfaced with Image Pro Plus as previously described (Guidi et al., 2013). Basal dendritic trees of Golgi-stained pyramidal neurons of layers II-III of the somatosensory cortex were traced live, at a final magnification of 500×, by focusing on the depth of the section. The operator starts with branches emerging from the cell soma and, after having drawn the first parent branch, goes on with all daughter branches of the next order in a centrifugal direction. At the end of tracing, the program reconstructs the number and length of individual branches, the mean length of branches of each order, and the total dendritic length.

2.4.2. Dendritic spine number and morphology

In Golgi-stained sections, dendritic spines located in the basal

dendrites of pyramidal neurons of layers II-III were manually counted using a 100× oil immersion objective lens (Leitz microscope and objective with 1.4 NA). For each mouse, 10 dendritic segments of 10 μm were analyzed and spine density was expressed as number of spines per 10 μm. Based on their morphology, dendritic spines can be divided into two different classes according to their state of maturation: immature and mature spines. The number of spines belonging to the 2 different groups (immature spines: filopodium-like, thin, and stubby-shaped; mature spines: mushroom- and cup-shaped) was counted and expressed as a percentage.

2.4.3. Analysis of neuronal soma size

Starting from images of Golgi-stained sections of the somatosensory cortex, the soma size of pyramidal neurons (area and major axes) was quantified by manually tracing the outline and short and long axes of neuronal soma with the software Image Pro Plus (Media Cybernetics, Silver Spring, MD 20910, USA) at a final magnification of 500×. A total of 40 pyramidal neurons per genotype at each age ($n = 10$ neurons per mouse, $n = 4$ mice per genotype at each age) of layers II-III of the somatosensory cortex was measured and analyzed.

2.4.4. Cell density

The number of Ki-67-positive cells was counted in the subgranular, granular layer, and hilus of the hippocampal dentate gyrus and expressed as number of cells/μm^2. DCX-positive cells were counted in the subgranular and granular layers of the dentate gyrus and expressed as number of neurons/100 μm. The number of Hoechst-positive nuclei in the upper granular layer of the dentate gyrus was manually counted and expressed as cells/μm^2.

2.4.5. Morphometric microglial cell analysis

Starting from 20× magnification images of AIF-1-stained cortical slices, the number of AIF-1-positive cells in the somatosensory cortex was manually counted using the point tool of the Image Pro Plus software (Media Cybernetics, Silver Spring, MD, USA), and cell density was established as AIF-1-positive cells/mm^3. AIF-1 positive microglial cell body size was manually drawn using the Image Pro Plus measurement function and was expressed in μm^2.

2.4.6. Quantification of VGluT1 and VGAT immunoreactive puncta

Images from the somatosensory cortex were acquired using a LEICA TCS SL confocal microscope (LEITZ; Leica Microsystems, Wetzlar, Germany; objective 63×, NA 1.32; zoom factor = 8). Three to four sections per animal were analyzed; in each section three images from the regions of interest were captured and the density of individual puncta exhibiting VGAT or VGluT1 immunoreactivity in layers II-III was evaluated as previously described in (Pizzo et al., 2016). The number of VGAT or VGluT1 immunoreactive puncta was expressed per μm^2.

2.5. Western blotting

For Western blot analysis tissue samples of the cortex were homogenized in RIPA buffer and quantified using the Bradford method, as previously described (Galvani et al., 2021). Equivalent amounts (50 μg) of protein were subjected to electrophoresis on a Bolt™ 4–12% Bis-Tris Plus gel (Life Technologies Corporation, Carlsbad, CA, USA) and transferred to a Hybond ECL nitrocellulose membrane (GE Healthcare Bio-Science, Piscataway, NJ, USA). The primary and secondary antibodies used are listed in Supplementary Table 1. The densitometric analysis of digitized Western blot images was performed using Chemidoc XRS Imaging Systems and the Image LabTM Software (Bio-Rad); this software automatically highlights any saturated pixels in the Western blot images in red. Images acquired with exposition times that generated protein signals out of a linear range were not considered for the quantification.

2.6. Behavioral testing

2.6.1. Surface righting

The righting reflex was tested using the Surface Righting Test in P5 mice, since this reflex appears in rodents at around this age (Heyser, 2004). As described in (Feather-Schussler and Ferguson, 2016) protocol, the pups were held on their backs on a cotton sheet; after 5 s they were released, and the time required to return to the prone position was recorded. A total time of 60 s was given for each trial, for a total of three trials.

2.6.2. Negative geotaxis

The Negative Geotaxis reflex was tested in P7 pups since this reflex appears in rodents at around this age (Heyser, 2004). As described in the (Feather-Schussler and Ferguson, 2016) protocol, the pups were placed heads downward on a 45° inclined plane and held in this position for 5 s. After this time, the pups were released, and the time they took to turn their faces upward was recorded. A total time of 120 s was given for each trial, for a total of three trials.

2.6.3. Cliff aversion

The Cliff Aversion test was performed on P8 mice following the protocol described in (Feather-Schussler and Ferguson, 2016). Pups were placed on top of a flat, elevated ledge, with only their forepaws and snout positioned over the edge. The total time taken for the pups to turn away from the cliff and move their paws and snout away from the edge was recorded. The test was repeated for a total of three trials.

2.7. Statistical analysis

The reported results are expressed as means ± standard error (SEM). The GraphPad Prism (version 7) software was used for data analysis. All datasets were analyzed using the ROUT method (Q = 1%) for the identification of significant outliers and the Shapiro-Wilk test for normality testing. Datasets with normal distribution were analyzed for significance using the two-tailed Student's *t*-test or two-way ANOVA, followed by Fisher's LSD post hoc test or Newman-Keuls multiple comparisons test, as specified in the figure legends. A probability level of $p < 0.05$ was considered to be statistically significant. The confidence level was taken as 95%. A descriptive statistic of genotype and age factors and Post-Hoc comparisons is given in Supplementary Table 2.

3. Results

3.1. Developmental changes in body weight in *Cdkl5* −/Y and *Cdkl5* +/Y mice

To assess whether defects in brain development due to loss of *Cdkl5* are already present at an early stage of life and to monitor their evolution with age, we analyzed *Cdkl5* −/Y mice at different ages (7-day-old, 14-day-old, 21-day-old, and 60-day-old mice). We first evaluated whether *Cdkl5* −/Y mice showed a significant difference in body weight compared to their wild-type counterparts. As previously reported in young and adult *Cdkl5* KO mice (Amendola et al., 2014), no genotype-related differences in body weight were observed between *Cdkl5* -/Y and wild-type mice at any of the analyzed ages (Table 1), showing evidence of similar physiological growth and no difference in food intake or animal well-being between *Cdkl5* −/Y and wild-type mice. In both genotypes, after an initial weight gain of +70 ±2.5% from P7 to P14, weight increased by a further +62 ±2.0% as mice progressed to adulthood (P60, Table 1).

3.2. Developmental changes in dendritic morphology in *Cdkl5* −/Y and *Cdkl5* +/Y mice

In order to establish whether defects in dendritic morphology are

Table 1
Body weight.

Age	Genotype	Body weight	n	p
P7	+/Y	4.66±0.13	16	n.s.
	-/Y	4.37±0.18	10	n.s.
P14	+/Y	7.76±0.14	16	n.s.
	-/Y	7.56±0.22	10	n.s.
P21	+/Y	9.10±0.20	25	n.s.
	-/Y	8.32±0.30	17	n.s.
P60	+/Y	19.66±0.63	14	n.s.
	-/Y	19.77±0.58	13	n.s.

Body weight in grams of wild-type (+/Y) and *Cdkl5* KO (−/Y) mice aged 7 (P7), 14 (P14), 21 (P21), and 60 (P60) days. Values are represented as mean ± SEM (Fisher's LSD test after two-way ANOVA); Abbreviations: n.s. = not significant; P = postnatal day.

already present at the earliest phases of brain development, we examined the basal dendritic tree of the pyramidal neurons in layer II/III of the somatosensory cortex (Fig. 1A) of *Cdkl5* −/Y mice. We first examined the number and mean length of segments, and the total length of the dendritic tree. Development of the dendritic tree consists of an increase in dendritic length and in the number of branches which leads to an increase in total dendritic length; dendrites branch more profusely and are spatially more expanded (Fig. 1B). Total dendritic tree size increased rapidly during the second postnatal week (from day 7 to day 14) in both wild-type and *Cdkl5* −/Y mice (Fig. 1C; +/Y +77.2±9.9%, −/Y +107±12.9%), due to an increase in both number and length of dendritic branches (Fig. 1D,C). The dendritic tree underwent a further increase to adulthood (day 60) (Fig. 1C; +/Y +38.7±11.04%, −/Y +47.7±3.01%, from day 14 to day 60). The number of dendritic segments per cell did not change during this time (Fig. 1D), but there was an increase in dendritic length (Fig. 1E). It is worth noting that, at all ages, *Cdkl5* -/Y mice had a reduced number (P7 –37±6.5%, P14 –23±3.3%, P21 –15±1.4%, P60 –23±1.8%) and length (P7 –30±2.7%, P14 –28 ±5.7%, P21 –16±5.5%, P60 –19±1.2%) of dendritic branches compared with wild-type (+/Y) mice (Fig. 1D,E), and a consequent reduction in total dendritic length (Fig. 1C).

In order to analyze dendritic morphology in detail we examined each dendritic order separately. As expected, there was an age-related increase in the maximum number of dendritic orders that, from a value of 5 in P7 and P14 wild-type mice, reached a value of 6 in P21 and P60 wild-type mice (Supplementary Fig. 1). In P7 and P14 mice there was no genotype-related difference in the maximum number of dendritic orders (Supplementary Fig. 1), while in P21 and P60 *Cdkl5* -/Y mice the branches of the last order (6) were missing (Supplementary Fig. 1). Regarding the mean length of dendritic branches of individual orders, we found few differences between wild-type and *Cdkl5* −/Y mice (Supplementary Fig. 1A-D). The only genotype-related differences regarded the mean length of branches of order 4 at P7 and of order 5 at P21 and P60, that were significantly smaller in *Cdkl5* −/Y mice in comparison with wild-type mice (Supplementary Fig. 1A-D). Regarding the number of dendritic branches of individual orders, we found significant differences, or a downward trend, in the number of ramifications in *Cdkl5* −/Y mice compared with wild-type mice, starting from order 2 (Supplementary Fig. 1E-H). Taken together, these results show early-appearing defects in the dendritic architecture of the pyramidal neurons of *Cdkl5* −/Y mice, represented by an overall reduction in the number and length of dendritic branches.

As an index of neuronal maturation (Miller and Peters, 1981), we evaluated the size of the cell body of the sampled pyramidal neurons (Fig. 1F). We found a difference between *Cdkl5* −/Y and wild-type mice in the long and short axes and in the surface area at P7, but not at more mature ages (Fig. 1G,H). The long axis was significantly smaller in *Cdkl5* −/Y mice in comparison with their wild-type counterparts, with a trend toward a reduction also in the short axis (Fig. 1G), and this, consequently, was also the case for the surface area (Fig. 1H). At all ages the ratio between the long and short axis was no different in *Cdkl5* -/Y mice in comparison with wild-type mice (Fig. 1I). Pyramidal neurons of both genotypes had an immature shape at P7 (Fig. 1I), as indicated by the smaller body size (Fig. 1G,H) and their more ovoid cell body (LA/SA closer to 1; Fig. 1I). At older ages, the soma of the pyramidal neurons of both *Cdkl5* -/Y and wild-type mice had a more pyramidal, mature shape (Fig. 1I).

3.3. Developmental changes in spine density and maturation in *Cdkl5* −/Y and *Cdkl5* +/Y mice

Spine density reduction is a typical feature of the dendritic pathology that affects the brain of adult *Cdkl5* -/Y mice (Fuchs et al., 2018; Fuchs et al., 2015; Trazzi et al., 2016). In addition, *Cdkl5* -/Y mice exhibit a deficit in dendritic spine structure and stabilization (Della Sala et al., 2016; Fuchs et al., 2018; Fuchs et al., 2015; Ricciardi et al., 2012; Trazzi et al., 2016). There is no information, however, regarding the onset of this defect. To this purpose, we examined the number of spines on the basal dendritic tree of the pyramidal neurons of the somatosensory cortex of *Cdkl5* −/Y mice (Fig. 2A,B). No differences between P7 *Cdkl5* −/Y and wild-type mice were present in spine density, indicating that during the early establishment of dendritic spines there are no genotype-related differences in their density (Fig. 2A,B). Differently, during the age-dependent increase in dendritic spine density, differences in the number of spines were present when comparing *Cdkl5* −/Y and wild-type mice (Fig. 2A,B). *Cdkl5* -/Y mice had a reduced spine density compared with their wild-type counterparts (Fig. 2A,B; P14 –7.8±1.2%, P21 –4.3±0.7%, P60 –8.3±1.0%). In wild-type mice the dendritic spine density on the cortical pyramidal neurons undergoes an age-related increase until adulthood (P60). Notably, from day 21 to day 60 this developmental increase in spine number was not present in *Cdkl5* -/Y mice, as spine density did not differ significantly over time (Fig. 2A,B).

Next, we categorized dendritic spines according to their morphologies to test whether the defect in spine formation in *Cdkl5* -/Y mice might be accompanied by an impairment in spine maturation represented by an overabundance of filopodia/thin and stubby spines. Therefore, similar to previous studies (Hering and Sheng, 2001), we categorized dendritic spines as filopodia-like and thin, stubby, mushroom-like, and cup spines. We found no differences in the percentage of mature spines between P7 *Cdkl5* -/Y and wild-type mice (Fig. 2A,C). The number of mature spines increased rapidly during the second postnatal week (from day 7 to day 14) in wild-type mice (Fig. 2C; +/Y +59±2.7%), but less so in *Cdkl5* -/Y mice (Fig. 2C;-/Y +22±9.9%), which led to a reduction in the percentage of mature spines in P14 *Cdkl5* -/Y (−52±3.2%) in comparison with wild-type mice (Fig. 2C). The lower percentage of mature spines was still present in P21 (−35±3.0%) and P60 (−32±1.5%) *Cdkl5* -/Y mice versus wild-type mice (Fig. 2A,C), indicating that the reduction in spine density was accompanied by alterations in spine maturation.

3.4. Developmental changes in glutamatergic and GABAergic axon terminals in *Cdkl5* −/Y and *Cdkl5* +/Y mice

Next, we investigated synaptic organization in the cortex of *Cdkl5* −/Y mice by analyzing the localization of the vesicular glutamate transporter 1 (VGluT1), which is a marker of cortico-cortical glutamatergic axon terminals (Wojcik et al., 2004), and that of the vesicular GABA transporter (VGAT), a marker of GABAergic axonal terminals (Chaudhry et al., 1998).

The density of VGluT1-positive puncta increased rapidly during the second postnatal week (from day 7 to day 14) in both wild-type and *Cdkl5* −/Y mice (Fig. 2D,F; +/Y +63.3±2.52%, −/Y +58.5±2.22%). Differently, while the density of VGluT1-positive puncta did not change with age in wild-type mice, it underwent a further increase during the third week (from day 14 to day 21) in *Cdkl5* -/Y mice (Fig. 2D,F; −/Y +15.9±2.12%). It is worth noting that, at all ages, *Cdkl5* -/Y mice had a

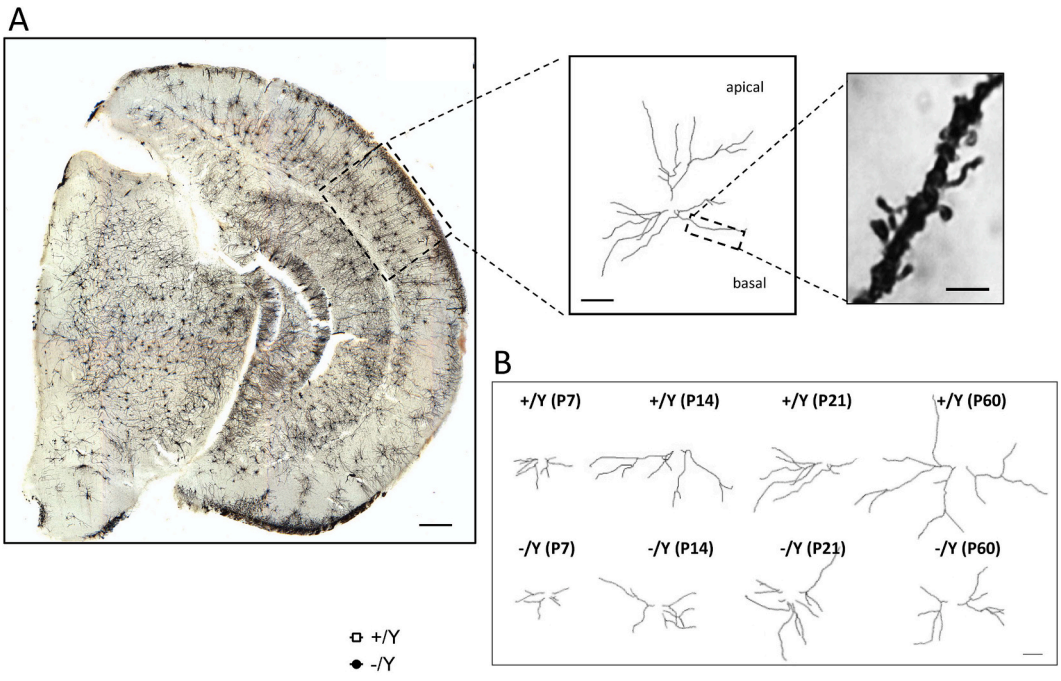

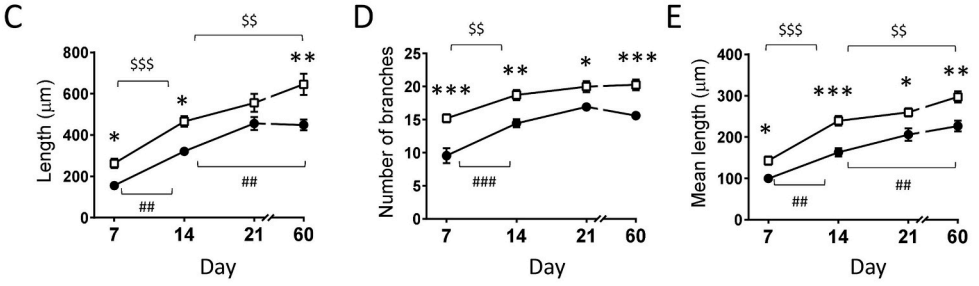

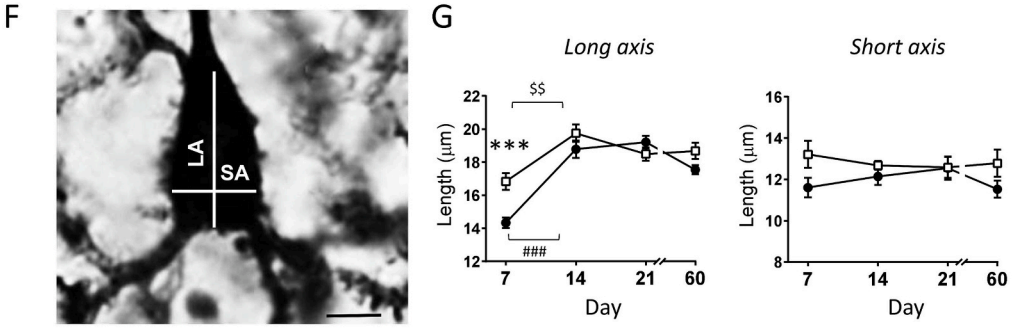

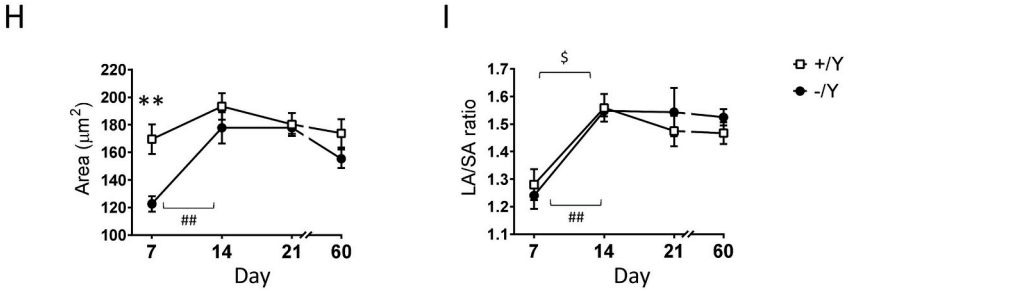

(caption on next page)

Fig. 1. Postnatal development of cortical pyramidal neurons in *Cdkl5* -/Y mice.
A: Representative image of a Golgi-stained section (panel on the left; scale bar = 500 μm), showing the cortical region of a P21 wild-type mouse in which the dendritic arbor of pyramidal neurons is traced (areas enclosed in the dashed square). In the middle is an example of the reconstructed apical and basal dendritic tree of a Golgi-stained cortical pyramidal neuron. Scale bar = 30 μm. In the image on the right is a Golgi-stained pyramidal neuron basal dendritic branch (areas enclosed in the dashed square) showing spines. Scale bar = 4 μm. B: Examples of the reconstructed basal dendritic tree of a Golgi-stained cortical pyramidal neuron of one wild-type (+/Y; upper) or *Cdkl5* -/Y (lower) mouse from each age group: P7, P14, P21, P60. Scale bar = 40 μm. C: Comparison between the total dendritic length of basal dendritic branches of Golgi-stained pyramidal neurons in the somatosensory cortex of *Cdkl5* +/Y and *Cdkl5* -/Y mice at 7 (P7), 14 (P14), 21 (P21) and 60 (P60) postnatal days of age. P7: *Cdkl5* +/Y *n* = 4; *Cdkl5* -/Y *n* = 3; P14: *Cdkl5* +/Y *n* = 4; *Cdkl5* -/Y n = 4; P21: *Cdkl5* +/Y n = 4; *Cdkl5* -/Y n = 4; P60: *Cdkl5* +/Y n = 4; *Cdkl5* -/Y *n* = 4. D,E: Number of branches (D) and mean length (E) of basal dendrites of cortical pyramidal neurons of mice as in C. F-G: Comparative analysis of the soma size of Golgi-stained pyramidal neurons in the somatosensory cortex of *Cdkl5* +/Y and *Cdkl5* -/Y mice. Representative image of a Golgi-stained cortical pyramidal neuron of a P21 wild-type mouse showing long (LA) and short (SA) somal axes in F. Scale bar = 6 μm. Graphs in G show the length of the long axis (on the left) and of the short axis (on the right) of wild-type (+/Y) and *Cdkl5* -/Y mice at different postnatal days of age. P7: *Cdkl5* +/Y n = 4; *Cdkl5* -/Y n = 4; P14: *Cdkl5* +/Y n = 4; *Cdkl5* -/Y *n* = 4; P21: *Cdkl5* +/Y n = 4; *Cdkl5* -/Y n = 4; P60: *Cdkl5* +/Y n = 4; *Cdkl5* -/Y *n* = 4. H-I: Somal area (H) and shape (I), expressed as LA/SA ratio, of pyramidal neurons in the cortex of mice as in G. Values in C-E and G-I are represented as means ± SEM. * $p < 0.05$, ** $p < 0.01$, *** $p < 0.001$ as compared to wild-type condition of the same age; $^{\#}$ $p < 0.05$, $^{\#\#}$ $p < 0.01$, $^{\#\#\#}$ $p < 0.001$ in the comparison between *Cdkl5* -/Y mice of different age groups; $^{\$}$ $p < 0.05$, $^{\$\$}$ $p < 0.01$, $^{\$\$\$}$ $p < 0.001$ in the comparison between *Cdkl5* +/Y mice of different age groups. Newman-Keuls test after two-way ANOVA. Abbreviations: LA = long axis; n = number of mice; P = postnatal day; SA = short axis.

higher density of VGluT1-positive puncta (P7 +10.9±0.14%, P14 +7.7 ±1.5%, P21 +27.9±2.34%, P60 +34.4±1.2%) compared with wild-type (+/Y) mice, a difference that increases with age (Fig. 2D,F).

Regarding inhibitory terminals, we found that, while density of VGAT-positive puncta in wild-type mice showed a variable trend in relation to age, with a rapid increase from P7 to P14 (Fig. 2E,F; +/Y +111.2±8.3%) and a subsequent decrease from P14 to P21 (Fig. 2E,F; +/Y −45.5±4.9%), *Cdkl5* -/Y mice showed a minor increment in inhibitory terminals from P7 to P14 (Fig. 2E,F; −/Y +14.9±2.0%) in comparison with wild-type mice, that was not followed by a subsequent reduction in later stages of development (Fig. 2E,F). At most developmental ages a higher density of VGAT-positive puncta was found in *Cdkl5* −/Y mice compared to their wild-type counterparts (Fig. 2E,F; P7 +32.8±4.4%, P21 +39.1±2.5%, P60 +28.8±2.9%), except for P14, an age at which *Cdkl5* −/Y mice showed a lower density of VGAT-positive puncta in comparison with wild-type mice of the same age (Fig. 2E,F; P14 −–27.6±1.2%).

Taken together, these data indicate a dysregulation of both glutamatergic and GABAergic terminal development in the cortex of *Cdkl5* −/Y mice.

3.5. Developmental changes in the density and morphology of microglia cells in Cdkl5 −/Y and Cdkl5 +/Y mice

Adult *Cdkl5* KO mice are characterized by increased microglial activation (Galvani et al., 2021; Medici et al., 2022), suggesting the involvement of inflammatory processes in the CDD pathophysiology. Young 20-day-old heterozygous female *Cdkl5* KO mice showed increased microglial body size compared to their wild-type counterparts of the same age, suggesting that microglia overactivation is an early onset defect (Galvani et al., 2021). To assess microglia overactivation, we analyzed microglial cell status by evaluating the density and analyzing the morphology of microglia (AIF-1-positive cells) in the cortex of all age groups in *Cdkl5* −/Y mice. In the early postnatal stage (first two weeks), microglial cells invade the brain from specific areas, such as the supraventricular corpus callosum (Hirasawa et al., 2005). These invading ameboid microglia migrate into the brain parenchyma where they ultimately mature into smaller body ramified microglia (Hirasawa et al., 2005). As development proceeds, the resident microglia decrease in number (Kim et al., 2015). As expected, in both *Cdkl5* -/Y and wild-type mice we found an increase in microglia cell density from day 7 to day 14 (Fig. 3A,B; +/Y +225±32%, −/Y +150±8.1%) and a significant decrease in the density of microglial cells with age (Fig. 3B; from day 14 to day 60, +/Y -39±2.3%, −/Y -24.5±1.5%). The minor decrease in microglial cells with age in *Cdkl5* -/Y mice likely subtends the higher density of microglia found in P60 *Cdkl5* −/Y mice in comparison to their wild-type counterparts (+19.4±2.4%; Student's *t*-test $p < 0.006$; Fig. 3B) (Galvani et al., 2021). Regarding microglial body size, a decrease in size, as an index of microglial maturation, was present in both *Cdkl5* −/Y and wild-type mice from day 7 to day 14 (Fig. 3A,C; +/Y -35.8±0.5%, −/Y -36±0.7%). Interestingly, microglial cells had an enlarged body size in all ages of *Cdkl5* -/Y mice compared to their wild-type counterparts of the same ages (Fig. 3C,D; P7 +23.6±4.6%, P14 +13.8±1.2%, P21 +12.8±1.5%, P60 +12.6±1.1%), indicating that in the absence of *Cdkl5*, the microglia adopted a larger soma shape, typical of a state of activation. Comparative analysis of microglia body size frequency distribution in *Cdkl5* −/Y mice versus age-matched wild-type mice confirmed the high percentage of microglia cells with a large body size in *Cdkl5* −/Y mice at each analyzed age, as showed by the right-shifted distribution compared to that of wild-type mice (Fig. 3D). While in the cortex of P7 mice of both genotypes the population of microglial cells had a greater body size variety (Fig. 3D), at later developmental stages microglia cells displayed cell bodies ranging in size from 40 to 120 μm^2 (Fig. 3D).

3.6. Developmental changes in hippocampal neurogenesis in Cdkl5 −/Y and Cdkl5 +/Y mice

Hippocampal neurogenesis plays a role in the maintenance and function of the dentate gyrus and hippocampal circuitry and consequently of cognitive functions (Kozareva et al., 2019). In terms of the process of neurogenesis, *Cdkl5* KO mice are characterized by an increased rate of apoptotic cell death of postmitotic granule precursors in the hippocampal dentate gyrus that causes a reduction in the final number of granule neurons (Fuchs et al., 2014). In order to establish whether the lack of Cdkl5 affects progenitor cell proliferation/survival in the hippocampal dentate gyrus (DG) at early developmental ages, immunohistochemistry for Ki-67, an endogenous marker of actively proliferating cells, and for doublecortin (DCX), a microtubule-associated protein expressed by differentiating (postmitotic) granule neurons, was performed on hippocampal slices. A quantitative analysis of the density of Ki-67-positive cells in the hippocampal dentate gyrus (granular layer (GL), subgranular zone (SGZ) and Hilus) showed that the pool of proliferating precursors in the DG rapidly decreased with age (Fig. 4A, B). *Cdkl5* −/Y mice had the same density of Ki-67 labeled cells as their wild-type counterparts of the same age, indicating no genotype-related difference in the number of proliferating precursors (Fig. 4A,B). As previously reported (Nicola et al., 2015), DCX-positive cells were not detectable at the earlier postnatal time point (P7 mice) since the DCX was poorly expressed in the newborn granule cells and was diffused throughout the DG (Supplementary Fig. 2). Quantification of DCX-positive cells in the GL of the DG showed that the density of newborn cells was notably lower in *Cdkl5* −/Y mice at all analyzed ages compared to their wild-type counterparts (Fig. 4C,D; P14 –12.7±3.4%, P21 –13.3 ±1.7%, P60 –29.5±9.1%), indicating that loss of *Cdkl5* affects survival of postmitotic neurons very early on during postnatal hippocampal

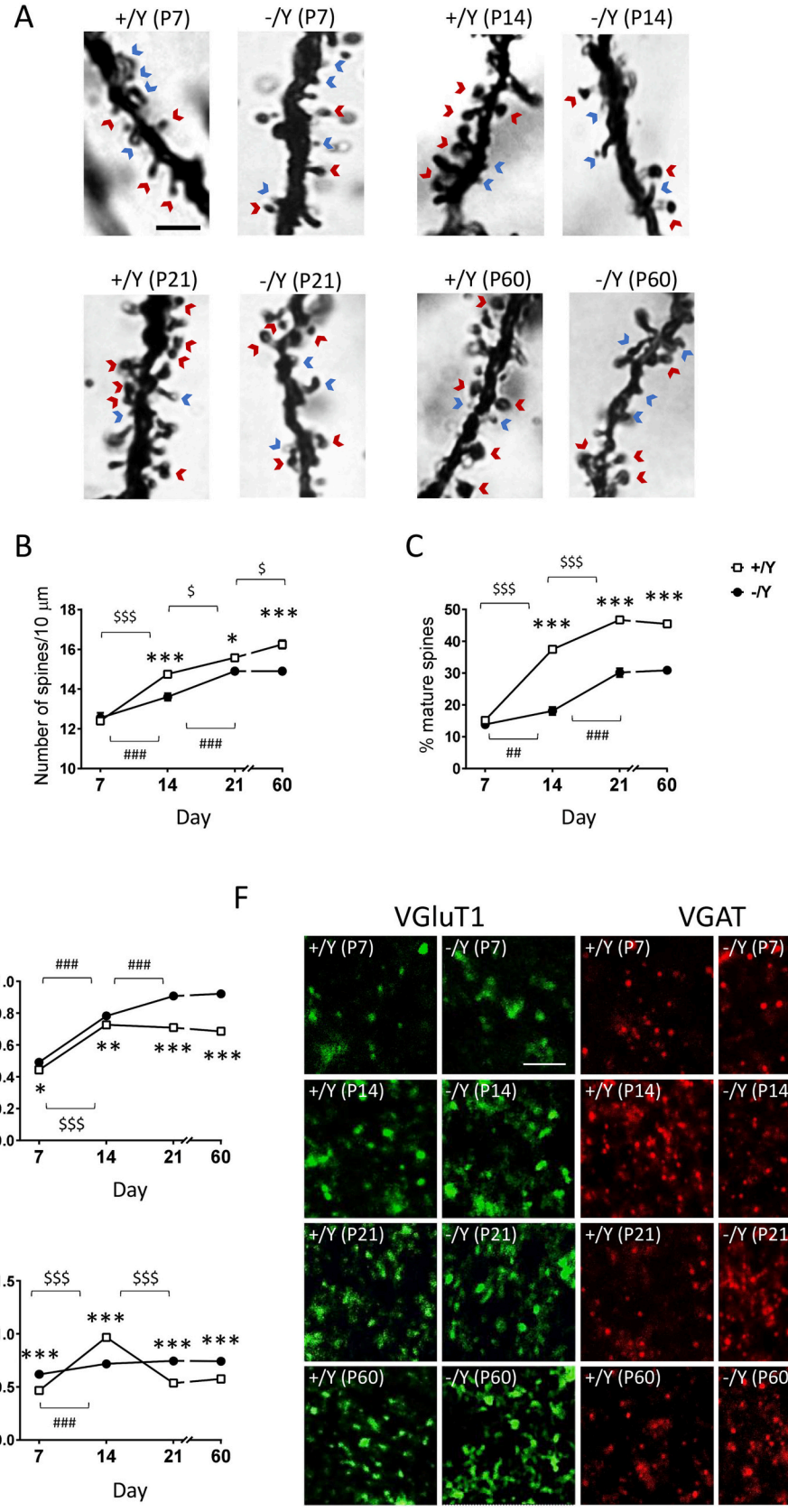

Fig. 2. Evolution of cortical dendritic spine maturation and neuronal connectivity during brain development in *Cdkl5* -/Y mice. A: Examples of Golgi-stained cortical pyramidal neurons of one animal from each experimental group; red arrows are examples of mature spines, blue arrows of immature spines. Scale bar = 4 µm. B: Comparison between spine density in basal dendrites of cortical pyramidal neurons of different age groups (P7: *Cdkl5* +/Y *n* = 4; *Cdkl5* -/Y n = 4; P14: *Cdkl5* +/Y n = 4; *Cdkl5* -/Y n = 4; P21: *Cdkl5* +/Y n = 4; *Cdkl5* -/Y n = 4; P60: *Cdkl5* +/Y n = 4; *Cdkl5* -/Y n = 4) of *Cdkl5* +/Y and *Cdkl5* -/Y mice. C: Percentage of mature dendritic spines in relation to the total number of protrusions in cortical pyramidal neurons of *Cdkl5* +/Y and *Cdkl5* -/Y mice as in B. D: Number of fluorescent puncta per µm^2 exhibiting vesicular glutamate transporter 1 (VGluT1) immunoreactivity in the somatosensory cortex of *Cdkl5* +/Y and *Cdkl5* -/Y mice of different age groups (P7: *Cdkl5* +/Y *n* = 3; *Cdkl5* -/Y n = 3; P14: *Cdkl5* +/Y n = 3; *Cdkl5* -/Y n = 3; P21: *Cdkl5* +/Y n = 3; *Cdkl5* -/Y n = 3; P60: *Cdkl5* +/Y n = 3; *Cdkl5* -/Y n = 3). E: Quantitative analysis of the number of vesicular GABA transporter (VGAT)-immunopositive puncta per µm^2 in the somatosensory cortex of *Cdkl5* +/Y and *Cdkl5* -/Y mice of different age groups as in D. F: Representative confocal images of cortical sections processed for VGluT1 immunohistochemistry (green) or VGAT immunohistochemistry (red) from a *Cdkl5* +/Y and a *Cdkl5* -/Y mouse at 7 (P7), 14 (P14), 21 (P21) and 60 (P60) postnatal days of age. Scale bar = 3 µm. Values in B-E are represented as means ± SEM. * $p < 0.05$, ** $p < 0.01$, *** $p < 0.001$ as compared to the wild-type condition of the same age; $^{\#\#}p < 0.01$, $^{\#\#\#}p < 0.001$ in the comparison between *Cdkl5* -/Y mice of different age groups; $^{\$}$ $p < 0.05$, $^{\$\$\$}$ $p < 0.001$ in the comparison between *Cdkl5* +/Y mice of different age groups. Newman-Keuls test after two-way ANOVA. Abbreviations: n = number of mice; P = postnatal day.

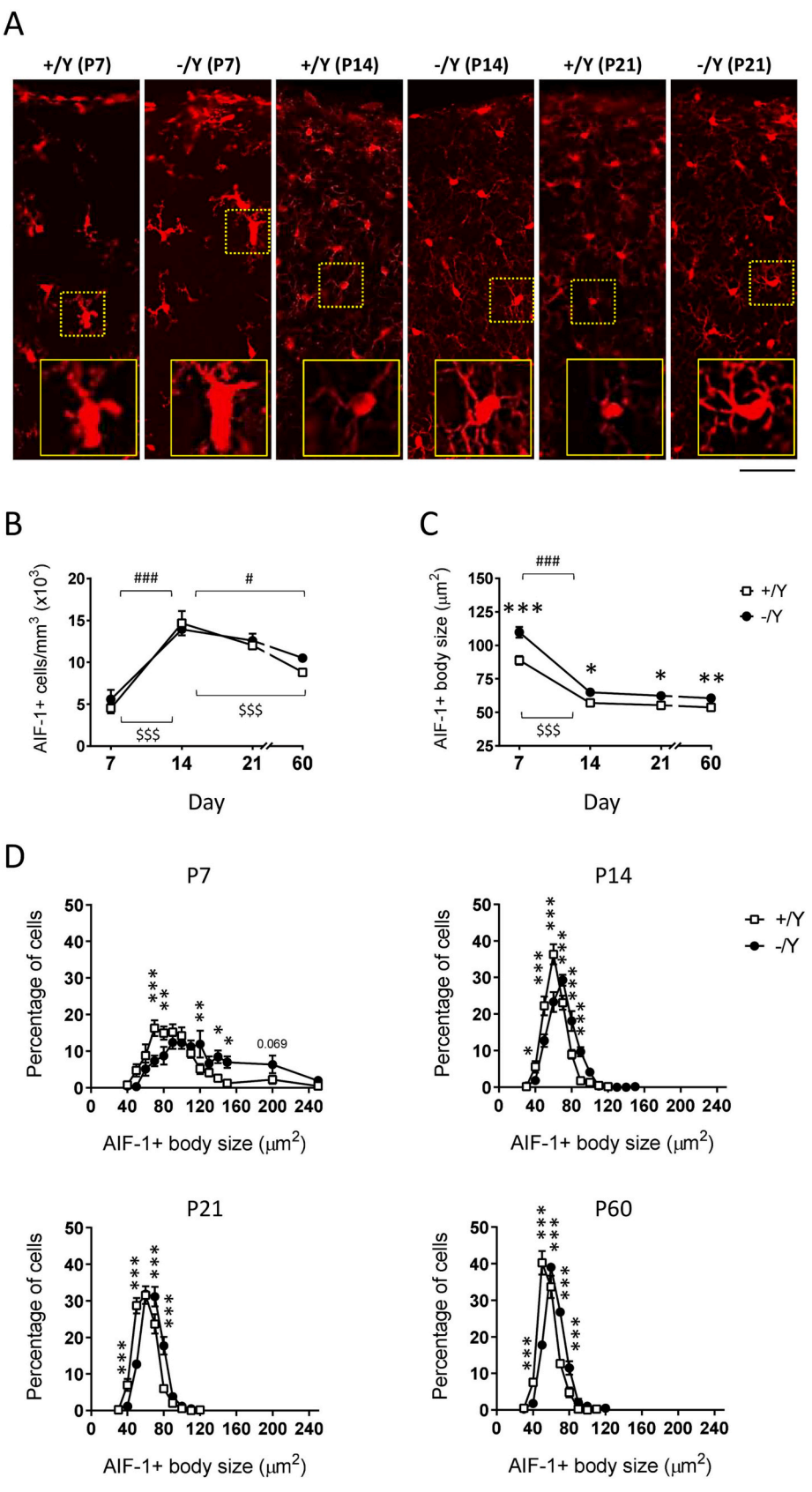

Fig. 3. Postnatal development of microglia density and body size in the cortex of *Cdkl5* -/Y mice.
A: Representative fluorescence images of cortical sections processed for AIF-1 immunohistochemistry of a wild-type (+/Y) and a *Cdkl5* KO mouse (−/Y) of different age groups. The dotted boxes in the upper panels indicate microglial cells shown in magnification in lower panels. High magnification (scale bar = 40 μm) and low magnification (scale bar = 10 μm). B: Quantification of AIF-1-positive cells in the cortex of *Cdkl5* +/Y and *Cdkl5* -/Y mice at 7 (P7), 14 (P14), 21 (P21), and 60 (P60) postnatal days of age. P7: *Cdkl5* +/Y *n* = 5; *Cdkl5* -/Y *n* = 4; P14: *Cdkl5* +/Y n = 4; *Cdkl5* -/Y n = 4; P21: *Cdkl5* +/Y n = 4; *Cdkl5* -/Y n = 5; P60: *Cdkl5* +/Y n = 4; *Cdkl5* -/Y n = 4. C: Mean microglia cell body size in somatosensory cortex sections from *Cdkl5* +/Y and *Cdkl5* -/Y mice; P7: *Cdkl5* +/Y n = 4; *Cdkl5* -/Y n = 4; P14: *Cdkl5* +/Y n = 4; *Cdkl5* -/Y n = 4; P21: *Cdkl5* +/Y n = 4; *Cdkl5* -/Y n = 4; P60: *Cdkl5* +/Y *n* = 8; *Cdkl5* -/Y *n* = 8. D: Distribution analysis of microglial cell soma area in the somatosensory cortex of *Cdkl5* +/Y and *Cdkl5* -/Y mice at 7 (P7), 14 (P14), 21 (P21), and 60 (P60) postnatal days of age as in B, showing a shift to larger cell body sizes in the absence of Cdkl5 at all ages. Data in B-D are presented as means ± SEM. * $p < 0.05$, ** $p < 0.01$, *** $p < 0.001$ as compared to the wild-type condition of the same age; $^{\#}$ $p < 0.05$, $^{\#\#\#}$ $p < 0.001$ in the comparison between *Cdkl5* -/Y mice of different age groups; $^{\$\$\$}$ $p < 0.001$ in the comparison between *Cdkl5* +/Y mice of different age groups. Newman-Keuls test after two-way ANOVA in B,C; Fisher's LSD test after two-way ANOVA in D. Abbreviations: n = number of mice; P = postnatal day.

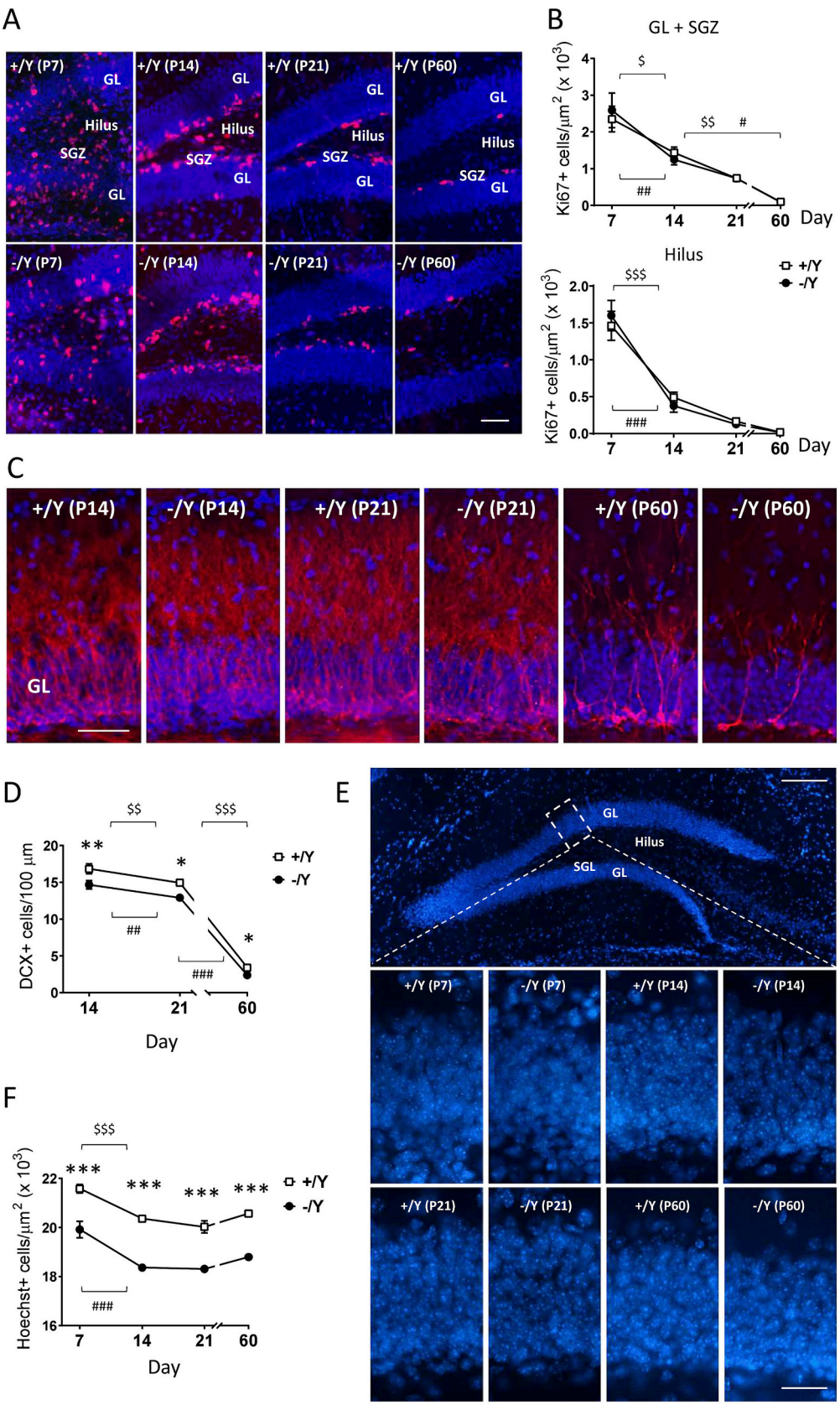

Fig. 4. Postnatal development of hippocampal neurogenesis in *Cdkl5* -/Y mice. A: Examples of sections processed for fluorescent Ki-67 immunostaining from the DG of one animal from each of the different age groups. Scale bar = 50 µm. B: Quantification of the number of Ki-67-positive cells in the GL plus SGL (upper graph) and in the dentate hilus (lower graph) of the DG of *Cdkl5* +/Y and *Cdkl5* -/Y mice at 7 (P7), 14 (P14), 21 (P21), and 60 (P60) postnatal days of age. P7: *Cdkl5* +/Y n = 5; *Cdkl5* -/Y n = 3; P14: *Cdkl5* +/Y n = 3; *Cdkl5* -/Y n = 3; P21: *Cdkl5* +/Y n = 3; *Cdkl5* -/Y n = 3; P60: *Cdkl5* +/Y n = 4; *Cdkl5* -/Y n = 4. C: Representative image of a DCX-immunostained section of the upper GL from the DG of one animal from each of the different age groups. Scale bar = 80 µm. D: Number of DCX-positive cells in the DG of different age groups (P14: *Cdkl5* +/Y n = 4; *Cdkl5* -/Y n = 4; P21: *Cdkl5* +/Y n = 3; *Cdkl5* -/Y n = 4; P60: *Cdkl5* +/Y *n* = 6; *Cdkl5* -/Y *n* = 7) of *Cdkl5* +/Y and *Cdkl5* -/Y mice. E: Representative image of a Hoechst-stained section (upper panel; scale bar = 100 µm), showing the portion of the DG in which the density of nuclei was quantified (areas enclosed in the dashed square). Lower panels: magnification of a section of the upper GL of the DG of a *Cdkl5* +/Y and *Cdkl5* -/Y mouse at 7 (P7), 14 (P14), 21 (P21), and 60 (P60) postnatal days of age. Scale bar = 30 µm. F: Quantification of Hoechst-positive cells in the GL of *Cdkl5* +/Y and *Cdkl5* -/Y mice of different age groups (P7: *Cdkl5* +/Y n = 4; *Cdkl5* -/Y n = 3; P14: *Cdkl5* +/Y n = 4; *Cdkl5* -/Y n = 4; P21: *Cdkl5* +/Y n = 4; *Cdkl5* -/Y n = 5; P60: *Cdkl5* +/Y n = 4; *Cdkl5* -/Y n = 4). Data are expressed as number of Hoechst-positive cells per µm^2. Values in B, D, and F are represented as means ± SEM. * $p < 0.05$, ** $p < 0.01$, *** $p < 0.001$ as compared to the wild-type condition of the same age; $^{\#}$ $p < 0.05$, $^{\#\#}$ $p < 0.01$, $^{\#\#\#}$ $p < 0.001$, in the comparison between *Cdkl5* -/Y mice of different age groups; $^{\$}$ $p < 0.05$, $^{\$\$}$ $p < 0.01$, $^{\$\$\$}$ $p < 0.001$ in the comparison between *Cdkl5* +/Y mice of different age groups. Newman-Keuls test after two-way ANOVA. Abbreviations: DG = dentate gyrus; GL = granular layer; n = number of mice; P = postnatal day; SGL = subgranular layer.

development.

To establish the impact of the reduced density of newly-formed granule neurons in *Cdkl5* −/Y mice on the overall granule cell number, we stereologically evaluated the granule cell number in mice. At all ages, we found a reduced granule cell density in *Cdkl5* −/Y mice compared to their wild-type counterparts (Fig. 4E,F; P7 –7.7±1.2%, P14 –9.7±0.6%, P21 –8.5±0.6%, P60 –8.6±0.3%), suggesting that a larger number of dying cells was already present in the GL of the DG of *Cdkl5* −/Y mice at a very early age.

3.7. Developmental changes in EB2 phosphorylation in the brain of *Cdkl5* −/Y and *Cdkl5* +/Y mice

Recent studies have suggested that CDKL5 plays a role in microtubule dynamics through its direct phosphorylation of microtubule-associated proteins such as end-binding 2 (EB2) protein (Baltussen et al., 2018), which may represent a potential molecular basis for the dendritic pathology exhibited by *Cdkl5* KO mice. In order to determine whether EB2 phosphorylation is dynamically regulated along with Cdkl5 throughout critical periods of brain development, we examined the protein levels of Cdkl5, phospho-EB2 (Ser22), and total EB2 at the various developmental mouse ages. While, as expected, Cdkl5 protein levels were undetectable at every age in *Cdkl5* −/Y mice cortex, in wild-type mice Cdkl5 levels slightly increased in adulthood (P60; Fig. 5A,B). Interestingly, phospho-EB2 levels were developmentally regulated, showing a substantial reduction between day 7 and day 14 in both wild-type and *Cdkl5* −/Y mice (Fig. 5A,C, +/Y -71.6±2.9%, −/Y -81.3 ±2.1%). The comparison of EB2 phosphorylation between *Cdkl5* −/Y and wild-type mice showed lower phospho-EB2 levels in *Cdkl5* −/Y mice brains at all ages (Fig. 5A,C; P7 –58.6±3.5%, P14 –59±7.9%, P21 –53.4 ±14%, P60 –88.2±4.9%). Interestingly, the percentage of reduction in EB2 phosphorylation in *Cdkl5* -/Y mice in comparison with their wild-type counterparts was higher in adult mice (P60), the age at which Cdkl5 is more greatly expressed, confirming a direct correlation between Cdkl5 activity and EB2 phosphorylation levels. Total levels of EB2 protein remained unchanged between day 7 and day 14 for both *Cdkl5* −/Y and wild-type mice showing instead a decreasing trend to P60 (Fig. 5A,D).

3.8. Early appearance of abnormal motor-reflex behavior responses in *Cdkl5* −/Y mice

Movement and coordination difficulties are the most common signs, along with delays in reaching motor developmental milestones in CDD children. To investigate the possible functional impact of the brain defects revealed in *Cdkl5* −/Y pups, we tested mice for motor ability (Surface Righting test) and labyrinth reflexes (Cliff Aversion test), as well as for strength and motor coordination (Cliff Aversion and Negative Geotaxis tests) (Fig. 6A). All these developmental tests require perception of body orientation in space. Righting reflex, negative geotaxis, and cliff drop aversion tests revealed a poorer performance of *Cdkl5* −/Y pups in comparison with their wild-type counterparts (Fig. 6B-D), indicating that developmental structural defects reflect altered behavior.

4. Discussion

This study demonstrates that most of the structural deficits of the brain in *Cdkl5* KO mice appear early during postnatal development (summarized in Supplementary Table 3). The earliest observed changes in 7-day-old mice include a reduction in the dendritic arbor of the pyramidal neurons, a deregulation in excitatory and inhibitory synaptic terminals, an increase in microglia activation, and a decrease in the survival of newborn hippocampal granule cells. A deficit in dendritic spines is not present in 7-day-old *Cdkl5* −/Y mice, but a reduction in dendritic spine density and maturation was observed in 14-day-old *Cdkl5* −/Y mice. These early defects are mostly retained during further stages of brain development, and do not worsen or improve with age, as *Cdkl5* −/Y and wild-type mice are characterized by similar age-related changes during postnatal brain development (Supplementary

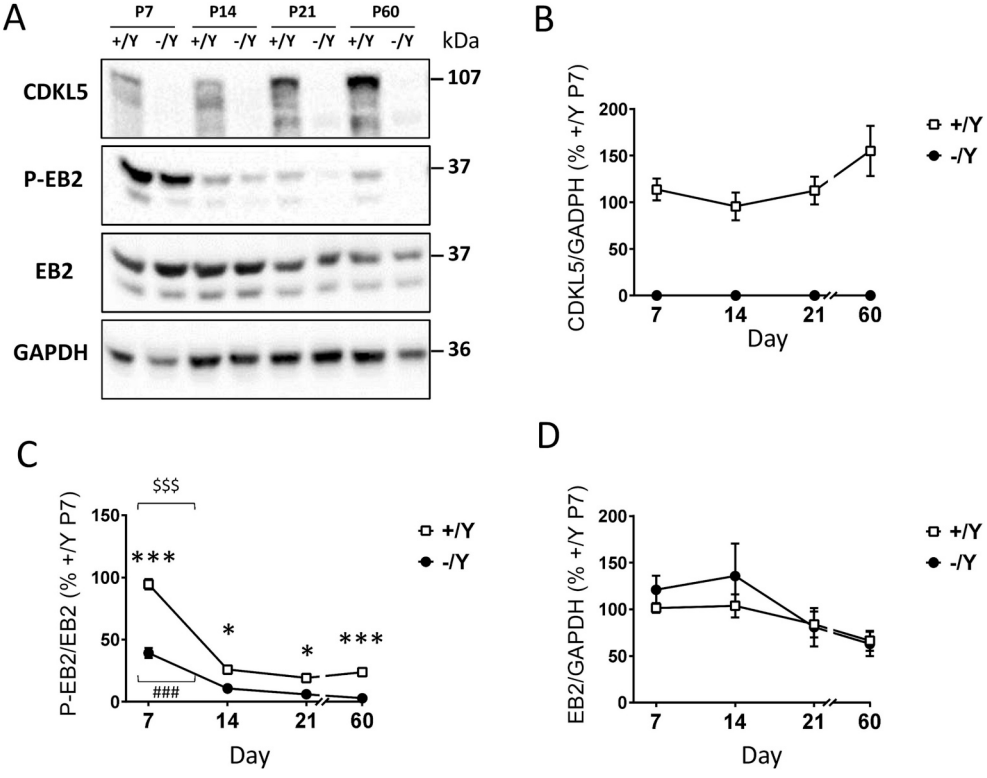

Fig. 5. Cdkl5, phospho-EB2, and EB2 levels in *Cdkl5* -/Y mice at different postnatal ages. A: Example of immunoblots from one animal of each experimental group. B-D: Western blot analysis of Cdkl5 (B), phospho-EB2 (P-EB2; C), and EB2 (D) levels in somatosensory cortex homogenates from *Cdkl5* +/Y and *Cdkl5* -/Y mice at 7 (P7), 14 (P14), 21 (P21), and 60 (P60) postnatal days of age. Graphs show Cdkl5 protein levels normalized to GAPDH in B (P7: *Cdkl5* +/Y $n = 11$; *Cdkl5* -/Y n = 4; P14: *Cdkl5* +/Y n = 11; *Cdkl5* -/Y n = 4; P21: *Cdkl5* +/Y n = 11; *Cdkl5* -/Y n = 4; P60: *Cdkl5* +/Y n = 11; *Cdkl5* -/Y n = 4), phospho-EB2 levels normalized to corresponding total EB2 protein levels in C, and EB2 levels normalized to GAPDH in D (P7: *Cdkl5* +/Y $n = 14$; *Cdkl5* -/Y n = 7; P14: *Cdkl5* +/Y n = 14; *Cdkl5* -/Y n = 7; P21: *Cdkl5* +/Y n = 14; *Cdkl5* -/Y n = 7; P60: *Cdkl5* +/Y n = 14; *Cdkl5* -/Y n = 8). Data are expressed as percentages of *Cdkl5* +/Y mouse levels at 7 days of age. Values are presented as means ± SEM; *$p < 0.05$, *** $p < 0.001$ as compared to the wild-type condition of the same age; ### $p < 0.001$ in the comparison between *Cdkl5* -/Y mice of different age groups; $$$ $p < 0.001$ in the comparison between *Cdkl5* +/Y mice of different age groups. Newman-Keuls test after two-way ANOVA. Abbreviations: n = number of mice; P = postnatal day.

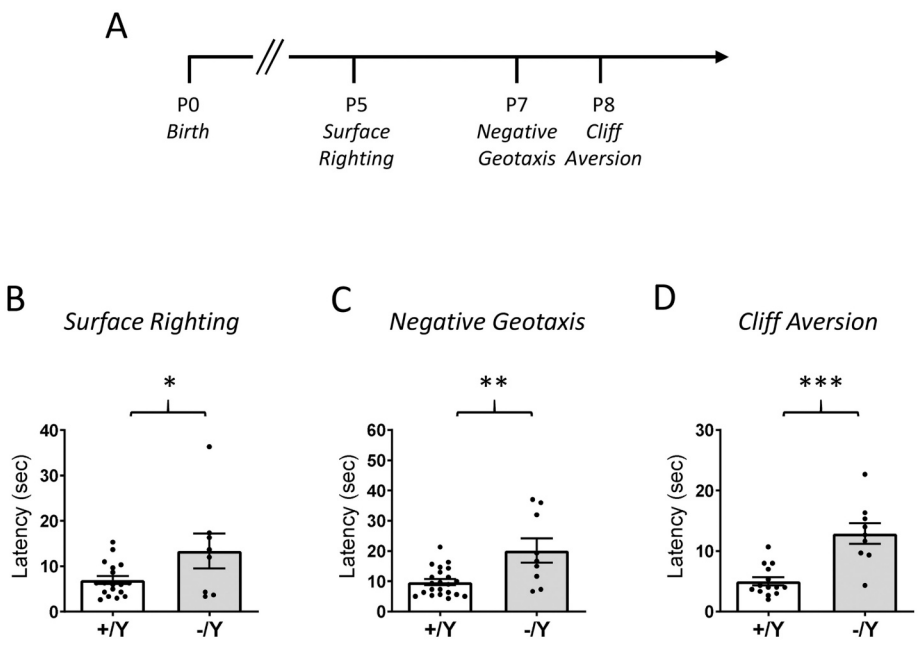

Fig. 6. Motor-reflexes in *Cdkl5* KO pups.
A: Timeline of when mice were behaviorally tested. The Surface Righting test was performed on postnatal day 5 (P5), the Negative Geotaxis test on postnatal day 7 (P7), and the Cliff Aversion test on postnatal day 8 (P8). B: Surface righting reflex in *Cdkl5* -/Y mice (n = 8) and wild-type littermates (+/Y *n* = 18). Histograms show the average time required for pups placed in the supine position to right themselves into the prone position. C: Abnormal negative geotaxis reflex in *Cdkl5* -/Y mice (*n* = 9) and control littermates (+/Y *n* = 22). Histograms show the latency of pups to turn and orient themselves facing up the slope. D: Cliff aversion reflex in *Cdkl5* -/Y mice (n = 9) and control littermates (+/Y n = 14). Graphs show the time required for pups to complete the reflex. The results in B-D are presented as means ± SEM. * $p < 0.05$, ** $p < 0.01$, *** $p < 0.001$ (two-tailed Student's *t*-test). Abbreviations: n = number of mice; P = postnatal day.

Table 4). Confirming the early presence of brain defects, *Cdkl5* −/Y pups (5–8 day-old mice) are characterized by an impairment in neonatal reflexes.

Dendritic arborization is significantly reduced in cortical pyramidal neurons from adult *Cdkl5* KO mice (Amendola et al., 2014; Ren et al., 2019). In the current study, we provide novel information regarding the appearance of dendritic abnormalities in the somatosensory cortex of a mouse model of CDD, the *Cdkl5* −/Y mouse. We found that at the end of the first week of age the dendritic tree of the pyramidal neurons of *Cdkl5* −/Y mice has a reduced number of branches and a reduced length. An analysis of the number and length of branches of each order showed differences between P7 *Cdkl5* −/Y and wild-type mice. These defects in dendritic complexity are retained during further stages of development, indeed, young (P14), juvenile (P21), and adult (P60) *Cdkl5* −/Y mice have cortical pyramidal neurons with a hypotrophic dendritic arbor in comparison with wild-type mice. These defects do not worsen with age, as seen in the similar age-related increase in the number and length of dendritic branches in both *Cdkl5* −/Y and wild-type mice.

The process of dendritogenesis is controlled by an intrinsic genetic program and extracellular signals (Urbanska et al., 2008). The mechanisms whereby the absence of Cdkl5 affects dendritic development remain elusive, although it is known that CDKL5 is not only required, but is sufficient to promote dendrite growth. It was previously shown that CDKL5 overexpression in SH-SY5Y neuroblastoma cells induces neurite outgrowth (Valli et al., 2012) and when overexpressed in cultured neurons, CDKL5 increased the total dendritic length (Chen et al., 2010), confirming that CDKL5 regulates a signaling pathway that controls dendrite growth. A recent study utilized iPSC derived neurons from patients with distinct mutations to show that loss of CDKL5 led to a decrease in phosphorylation of the CDKL5 substrate EB2. As a microtubule regulator, EB2 phosphorylation status was shown to be critical for microtubule dynamics within dendrites (Baltussen et al., 2018), suggesting that EB2 phosphorylation levels were involved in dendritic outgrowth. In support of this, as previously reported (Baltussen et al., 2018), we found a reduction of phospho-EB2 levels in the mouse cortex with age, which links EB2 phosphorylation to the developmental time of neurite outgrowth. Specific studies are required to determine the role of phospho-EB2 and, possibly, other pathways in the regulation of dendritic development at different developmental time points in the *Cdkl5* KO brain.

The cell bodies of pyramidal neurons change markedly as pyramidal neurons mature. Not only does the shape of the cell body transform from a spheroid to a more pyramidal shape, but the size of the soma increases substantially in the first few weeks after birth (Miller and Peters, 1981). Interestingly, pyramidal neurons of the somatosensory cortex had a soma with a smaller size in P7 *Cdkl5* −/Y mice versus their wild-type counterparts, subtending a reduced neuronal maturation in the absence of Cdkl5 which also involves the soma size of the pyramidal neurons. However, differently from the dendritic arbor, the soma size defect changes over time and it is not retained during further stages of development. In *Cdkl5* −/Y mice, probably due to some form of compensation that takes place between P7 and P14, the cell body of *Cdkl5* −/Y pyramidal neurons no longer differs from that of wild-type counterparts of the same age.

Alterations in spine density and maturation correspond with aberrant brain function observed in various neurodevelopmental and neuropsychiatric disorders (Khanal and Hotulainen, 2021). Various studies in vitro and in vivo converge regarding the role of CDKL5 in controlling dendritic spine morphology and excitatory functions (Barbiero et al., 2019). Previous evidence showed differences in dendritic spine density and maturation of cortical pyramidal cells in juvenile (P27–P28) and adult *Cdkl5* KO in comparison with wild-type mice (Della Sala et al., 2016; Ren et al., 2019). Neurons that are devoid of CDKL5 are characterized by an increased number of filopodia-like protrusions and a reduced number of mushroom-shaped spines (Della Sala et al., 2016; Ricciardi et al., 2012). The enlarged spine heads, which are distinguished by their mushroom-shaped spines, correlate with increased synaptic strength. Importantly, an alteration in dendritic spine formation was also observed in neurons derived from induced pluripotent stem cells reprogrammed from patient fibroblasts, suggesting that spine and synaptic abnormalities are also likely to be present in patients (Ricciardi et al., 2012).

We found no differences between P7 *Cdkl5* −/Y and wild-type mice in the density of dendritic spines as well as in the percentage of mature spines. In contrast, an evaluation of basal dendritic spines in *Cdkl5* −/Y mice at later ages showed genotype-related differences. Spines are dynamic structures and their shape, size, and density change with developmental age and depend upon the balance among spine initiation, stabilization, and pruning rate. The evidence that in the cortex of *Cdkl5* −/Y mice new spines are normally generated (spine initialization) but

fail to stabilize (spine maturation), and are eliminated (spine pruning) at an abnormally high rate (Della Sala et al., 2016) may explain our finding that in 7-day-old *Cdkl5* −/Y neurons, which have mainly immature spines (86%), differences in spine density are still not present.

Taken together our results show that, while very precocious defects are present in the basal dendritic arbor of pyramidal neurons in *Cdkl5* −/Y mice, defects in spine density and maturation start to appear slightly later in development. This suggests that defects in spine development due to lack of Cdkl5 are temporally shifted in relation to the process of dendritogenesis.

Absence of CDKL5 profoundly affects not only the number of spines, the postsynaptic sites for excitatory synapses, but also the excitatory and inhibitory presynaptic terminals (Pizzo et al., 2016). As expected, since synaptogenesis occurs largely during the first postnatal period in rodents, with the greatest increases in synaptic density during the phase of the greatest synaptogenesis (P11–P16 in the mouse), we found an increase in the density of excitatory and inhibitor terminals from P7 to P14 in both *Cdkl5* −/Y and wild-type mice. However, the development of the number and stabilization of synaptic terminals was not the same in *Cdkl5* −/Y and in wild-type mice. A higher number of putative excitatory terminals labeled for VGluT1 had previously been observed in the cortex of adult *Cdkl5* −/Y mice compared to their wild-type counterparts (Pizzo et al., 2016). In agreement with this finding we found a higher density of excitatory terminals in the cortex of *Cdkl5* −/Y mice at all analyzed ages. However, the difference in the density of excitatory terminals between *Cdkl5* KO and wild-type mice increases with age. This could be attributed to an increase in callosal excitatory synaptic inputs with age — indeed, a functional hyperconnectivity across hemispheres has been described in *Cdkl5* KO mice (Awad et al., 2023) — and/or to a compensatory mechanism established to counteract reduced postsynaptic functionality (number of mature spines). In addition to changes regarding the glutamatergic terminals, we found an increased density of GABAergic terminals in *Cdkl5* −/Y mice. Our finding that in the wild-type cortex the density of inhibitor terminals increased from P7 to P14, and then decreased by 44% to P21 and adult levels, is in line with the finding that in the rat visual cortex symmetrical synapses (putatively inhibitory synapses) decline significantly following the second/third week after birth (Blue and Parnavelas, 1983). This decline was also evident in the somatosensory cortex of the mouse, but occurred after P32 (De Felipe et al., 1997), indicating that the inhibitory synapses are affected by the pruning process. Interestingly, we found an increased density of GABAergic axonal boutons in the cortex of *Cdkl5* −/Y mice during postnatal development at P7 and P21 and in adulthood; however, fewer inhibitory terminals were present at P14, in comparison with their age-matched wild-type counterpart. We can hypothesize that, in the absence of Cdkl5, the period of the high rate of production of new inhibitory synapses does not occur or lasts for a briefer time, inhibiting the transient increase in the number of inhibitory synapses. The mechanisms responsible for the age-related increased density or pruning of inhibitory terminals in *Cdkl5* −/Y mice are presently unclear. However, CDKL5 was reported to be expressed at high levels in GABAergic interneurons (Rusconi et al., 2008), suggesting a possible involvement of Cdkl5 in the kinetic of synaptogenesis of the inhibitory neurons. A study aimed at evaluating the inhibitory and excitatory postsynaptic currents will be an important future step to determine age-related synaptic function alterations in the absence of CDKL5.

Microglia activation, associated with an increase in cell body size, as well as with cytokine alterations, has recently been described in *Cdkl5* KO mice (Galvani et al., 2021). Our results highlight the presence of a generalized status of microglia overactivation in the brain of the *Cdkl5* −/Y mouse, that is already present at a very early stage of life. As previously described (Lawson et al., 1990; Perry et al., 1985), we observed that during postnatal brain development in the mouse microglia gradually accumulate, dramatically increasing in number between P7 and P14; by P14, the entire cortical parenchyma is filled with ramified microglia. Microglia make essential contributions to CNS development. They regulate neurogenesis and neuronal migration in addition to facilitating neural connectivity by regulating axon outgrowth, myelination, and remodeling synaptic connections (Frost and Schafer, 2016; Li and Barres, 2018; Sato, 2015; Tremblay et al., 2010). Interestingly, in the developing brain, microglia interact specifically with neuronal synapses, thus influencing synaptic maturation and pruning (Parkhurst et al., 2013; Tremblay et al., 2010). Our previous finding that inhibition of neuroinflammation through treatment with luteolin improves dendritic pathology in (3–4-month-old) *Cdkl5* +/− female mice (Tassinari et al., 2022) strongly suggests that an inflammatory state is associated with the pathophysiology of the adult CDD brain. The early arrival of microglia in the developing brain, together with the presence of an activated phenotype in the absence of Cdkl5, suggests a possible developmental microglia-neuron crosstalk that may affect neuronal maturation and survival in the *Cdkl5* null brain at a very early age.

The majority of the immature granule neurons, derived from primary progenitor cells located in the subgranular layer of the dentate gyrus (DG), are subjected to a selection process, during which they are either recruited into function or eliminated (Biebl et al., 2000). Cdkl5 loss causes hypocellularity of the DG due to the increased apoptotic cell death of immature granule neurons (DCX+ cells) that overrides the proliferation of their progenitors (Fuchs et al., 2014). Here we found that loss of Cdkl5 already decreases survival of postmitotic neurons very early on in postnatal hippocampal development. There is evidence that activated microglia, through the integrin CD11b in cooperation with the immunoreceptor DAP12, trigger developmental apoptosis of hippocampal neurons via the production of superoxide ions (Wakselman et al., 2008). It is therefore possible that Cdkl5 loss-induced microglia activation could also lead to excessive immature newborn neuronal death. Future studies aimed at evaluating the effect of the inhibition of neuroinflammation during the early phase of brain development in *Cdkl5* KO mice will help to clarify whether microglia activation underlies early postnatal structural deficits in the *Cdkl5* null brain.

Our finding that most of the reported brain alterations appear to be already well established in 7-day-old *Cdkl5* pups suggests a very early onset of these defects. However, we are aware that there are limitations to our study. First, we did not identify at what stage, before 7 days of age, the brain defects appear in *Cdkl5* −/Y mice. Second, the behavioral analysis was carried out within a limited time window (5–8 days). Therefore, even if this analysis supports the presence of early behavioral alterations, it does not allow us to identify the onset of behavioral defects and their temporal progression. Considering that CDKL5 is expressed in foetal brains both in humans and mice (Hector et al., 2016), future studies of brain development/function during perinatal and prenatal ages in *Cdkl5* KO mice will provide indications regarding the onset and progression of brain alterations. In addition, although most CDD patients are females who are heterozygous for CDKL5 deficiency, in this first comparative study of brain development in the early postnatal period through adulthood we used, as a CDD disease model, *Cdkl5* −/Y male mice. A study aimed at characterizing brain development in *Cdkl5* +/− females will be an important future step that will help to clarify the complex CDD pathophysiological processes in a context in which the mosaicism of Cdkl5 expression could influence the phenotypic outcome.

5. Conclusions

Taken together, the current findings show that dendritic pathology, the main cause of behavioral defects such as motor and cognitive disability, is detectable very early on in the brain of *Cdkl5* −/Y pups. Similarly, a decreased survival of postmitotic neurons that causes hypocellularity of the DG appears early in the postnatal developing brain, probably compromising the function of the hippocampal circuit. Both humans and rodents undergo extensive postnatal neurological development, and have a relatively immature CNS at birth (Zeiss, 2021). The primary developmental events occurring postnatally in humans are synapse production, myelination, and neuronal and synaptic pruning. In

general, the same processes occur in rodents. For example, maximum brain growth occurs after birth both in humans and rodents, and a significant amount of synaptogenesis continues postnatally. Although postnatal development of CNS is not identical between humans and rodents — there are examples in which the human is more developed at birth than rodents, such as neurogenesis in the dentate gyrus (Zeiss, 2021) — rodents appear to be an appropriate model for evaluating genotype-related effects on postnatal brain development in humans (Watson et al., 2006). Therefore, even if knowledge of the timeline of dendritic pathology in CDD patients is still missing, the current findings strengthen the suitability of the mouse model of CDD as a tool to test early therapeutic interventions aimed at ameliorating brain development and, therefore, intellectual disability in children with CDD.

Author contributions

EC designed the study. MT, BU, and ST performed the experiments and analyzed the data with support from CC, OC, NM, ML, GC, and GM; EC and ST wrote the manuscript. All authors approved the final manuscript.

CRediT authorship contribution statement

Marianna Tassinari: Investigation, Visualization, Methodology, Data curation, Writing – review & editing. **Beatrice Uguagliati:** Investigation, Visualization, Methodology, Data curation, Writing – original draft. **Stefania Trazzi:** Investigation, Visualization, Formal analysis, Data curation, Writing – original draft, Writing – review & editing. **Camilla Bruna Cerchier:** Investigation, Resources, Writing – review & editing. **Ottavia Vera Cavina:** Investigation, Writing – review & editing. **Nicola Mottolese:** Resources, Writing – review & editing. **Manuela Loi:** Validation, Resources, Writing – review & editing. **Giulia Candini:** Resources, Writing – review & editing. **Giorgio Medici:** Resources, Writing – review & editing. **Elisabetta Ciani:** Conceptualization, Visualization, Formal analysis, Data curation, Writing – original draft, Writing – review & editing, Supervision, Project administration, Funding acquisition.

Declaration of Competing Interest

The authors declare no conflict of interests related to this article.

Data availability

Data will be made available on request.

Acknowledgments

This work was supported by a contribution from the Italian parent association “CDKL5 insieme verso la cura” and from the Ministry of University and Research (MUR), National Recovery and Resilience Plan (NRRP), NEXTGENERATIONEU, project MNESYS (PE0000006) to EC. We thank Dr. Domenico Ferrara for the technical support.

Appendix A. Supplementary data

Supplementary data to this article can be found online at https://doi.org/10.1016/j.nbd.2023.106146.

Bibliography

Amendola, E., et al., 2014. Mapping pathological phenotypes in a mouse model of CDKL5 disorder. PLoS One 9, e91613.
Awad, P.N., et al., 2023. CDKL5 sculpts functional callosal connectivity to promote cognitive flexibility. Mol. Psychiatry. 1–12.
Bahi-Buisson, N., Bienvenu, T., 2012. CDKL5-related disorders: from clinical description to molecular genetics. Mol. Syndromol. 2, 137–152.
Baltussen, L.L., et al., 2018. Chemical genetic identification of CDKL5 substrates reveals its role in neuronal microtubule dynamics. EMBO J. 37, 1–19.
Barbiero, I., et al., 2019. Microtubules: a key to understand and correct neuronal defects in CDKL5 deficiency disorder? Int. J. Mol. Sci. 20, 4075–4093.
Biebl, M., et al., 2000. Analysis of neurogenesis and programmed cell death reveals a self-renewing capacity in the adult rat brain. Neurosci. Lett. 291, 17–20.
Blue, M.E., Parnavelas, J.G., 1983. The formation and maturation of synapses in the visual cortex of the rat. II. Quantitative analysis. J. Neurocytol. 12, 697–712.
Chaudhry, F.A., et al., 1998. The vesicular GABA transporter, VGAT, localizes to synaptic vesicles in sets of glycinergic as well as GABAergic neurons. J. Neurosci. 18, 9733–9750.
Chen, Q., et al., 2010. CDKL5, a protein associated with rett syndrome, regulates neuronal morphogenesis via Rac1 signaling. J. Neurosci. 30, 12777–12786.
De Felipe, J., et al., 1997. Inhibitory synaptogenesis in mouse somatosensory cortex. Cereb. Cortex 7, 619–634.
Della Sala, G., et al., 2016. Dendritic spine instability in a mouse model of CDKL5 disorder is rescued by insulin-like growth factor 1. Biol. Psychiatry 80, 302–311.
Eller, K., et al., 1969. Ontogeny of the mouse motor cortex. The polymorph layer or layer VI. A Golgi and electronmicroscopical study. Z Zellforsch Mikrosk Anat. 99, 443–458.
Feather-Schussler, D.N., Ferguson, T.S., 2016. A battery of motor tests in a neonatal mouse model of cerebral Palsy. J. Vis. Exp. 117, 53569–53581.
Frost, J.L., Schafer, D.P., 2016. Microglia: architects of the developing nervous system. Trends Cell Biol. 26, 587–597.
Fuchs, C., et al., 2014. Loss of CDKL5 impairs survival and dendritic growth of newborn neurons by altering AKT/GSK-3beta signaling. Neurobiol. Dis. 70, 53–68.
Fuchs, C., et al., 2015. Inhibition of GSK3beta rescues hippocampal development and learning in a mouse model of CDKL5 disorder. Neurobiol. Dis. 82, 298–310.
Fuchs, C., et al., 2018. Treatment with the GSK3-beta inhibitor Tideglusib improves hippocampal development and memory performance in juvenile, but not adult, Cdkl5 knockout mice. Eur. J. Neurosci. 47, 1054–1066.
Galvani, G., et al., 2021. Inhibition of microglia over-activation restores neuronal survival in a mouse model of CDKL5 Deficent disorder. J. Neuroinflammation 18, 155–176.
Gennaccaro, L., et al., 2021. Age-related cognitive and motor decline in a mouse model of CDKL5 deficiency disorder is associated with increased neuronal senescence and death. Aging Dis. 12, 764–785.
Guidi, S., et al., 2013. Early pharmacotherapy with fluoxetine rescues dendritic pathology in the Ts65Dn mouse model of down syndrome. Brain Pathol. 23, 129–143.
Hector, R.D., et al., 2016. Characterisation of CDKL5 transcript isoforms in human and mouse. PLoS One 11, e0157758.
Hering, H., Sheng, M., 2001. Dendritic spines: structure, dynamics and regulation. Nat. Rev. Neurosci. 2, 880–888.
Heyser, C.J., 2004. Assessment of developmental milestones in rodents. In: Curr Protoc Neurosci. Chapter 8, Unit 8, p. 18.
Hirasawa, T., et al., 2005. Visualization of microglia in living tissues using Iba1-EGFP transgenic mice. J. Neurosci. Res. 81, 357–362.
Jakimiec, M., et al., 2020. CDKL5 deficiency disorder-a complex epileptic encephalopathy. Brain Sci. 10.
Juraska, J.M., Fifkova, E., 1979. A Golgi study of the early postnatal development of the visual cortex of the hooded rat. J. Comp. Neurol. 183, 247–256.
Khanal, P., Hotulainen, P., 2021. Dendritic spine initiation in brain development, learning and diseases and impact of BAR-domain proteins. Cells 10, 2392–2417.
Kim, I., et al., 2015. A postnatal peak in microglial development in the mouse hippocampus is correlated with heightened sensitivity to seizure triggers. Brain Behav. 5, e00403.
Kozareva, D.A., et al., 2019. Born this way: hippocampal neurogenesis across the lifespan. Aging Cell 18, e13007.
Lawson, L.J., et al., 1990. Heterogeneity in the distribution and morphology of microglia in the normal adult mouse brain. Neuroscience. 39, 151–170.
Li, Q., Barres, B.A., 2018. Microglia and macrophages in brain homeostasis and disease. Nat. Rev. Immunol. 18, 225–242.
Loi, M., et al., 2020. Increased DNA damage and apoptosis in CDKL5-deficient neurons. Mol. Neurobiol. 57, 2244–2262.
Lopez-Rivera, J.A., et al., 2020. A catalogue of new incidence estimates of monogenic neurodevelopmental disorders caused by de novo variants. Brain. 143, 1099–1105.
Medici, G., et al., 2022. Expression of a Secretable, cell-penetrating CDKL5 protein enhances the efficacy of gene therapy for CDKL5 deficiency disorder. Neurotherapeutics 19, 1886–1904.
Miller, M., Peters, A., 1981. Maturation of rat visual cortex. II. A combined Golgi-electron microscope study of pyramidal neurons. J. Comp. Neurol. 203, 555–573.
Nicola, Z., et al., 2015. Development of the adult neurogenic niche in the hippocampus of mice. Front. Neuroanat. 9, 53.
Okuda, K., et al., 2017. CDKL5 controls postsynaptic localization of GluN2B-containing NMDA receptors in the hippocampus and regulates seizure susceptibility. Neurobiol. Dis. 106, 158–170.
Olson, H.E., et al., 2019. Cyclin-dependent kinase-like 5 deficiency disorder: clinical review. Pediatr. Neurol. 97, 18–25.
Parkhurst, C.N., et al., 2013. Microglia promote learning-dependent synapse formation through brain-derived neurotrophic factor. Cell. 155, 1596–1609.
Perry, V.H., et al., 1985. Immunohistochemical localization of macrophages and microglia in the adult and developing mouse brain. Neuroscience. 15, 313–326.
Pizzo, R., et al., 2016. Lack of Cdkl5 disrupts the organization of excitatory and inhibitory synapses and parvalbumin interneurons in the primary visual cortex. Front. Cell. Neurosci. 10, 261–277.

Ren, E., et al., 2019. Functional and structural impairments in the Perirhinal cortex of a mouse model of CDKL5 deficiency disorder are rescued by a TrkB agonist. Front. Cell. Neurosci. 13, 169–184.
Ricciardi, S., et al., 2012. CDKL5 ensures excitatory synapse stability by reinforcing NGL-1-PSD95 interaction in the postsynaptic compartment and is impaired in patient iPSC-derived neurons. Nat. Cell Biol. 14, 911–923.
Rusconi, L., et al., 2008. CDKL5 expression is modulated during neuronal development and its subcellular distribution is tightly regulated by the C-terminal tail. J. Biol. Chem. 283, 30101–30111.
Sato, K., 2015. Effects of microglia on neurogenesis. Glia. 63, 1394–1405.
Symonds, J.D., et al., 2019. Incidence and phenotypes of childhood-onset genetic epilepsies: a prospective population-based national cohort. Brain. 142, 2303–2318.
Tassinari, M., et al., 2022. Luteolin treatment ameliorates brain development and behavioral performance in a mouse model of CDKL5 deficiency disorder. Int. J. Mol. Sci. 23, 8719–8743.
Trazzi, S., et al., 2016. HDAC4: a key factor underlying brain developmental alterations in CDKL5 disorder. Hum. Mol. Genet. 25, 3887–3907.
Tremblay, M.E., et al., 2010. Microglial interactions with synapses are modulated by visual experience. PLoS Biol. 8, e1000527.
Urbanska, M., et al., 2008. Molecular basis of dendritic arborization. Acta Neurobiol. Exp. (Wars) 68, 264–288.
Valli, E., et al., 2012. CDKL5, a novel MYCN-repressed gene, blocks cell cycle and promotes differentiation of neuronal cells. Biochim. Biophys. Acta 1819, 1173–1185.
Wakselman, S., et al., 2008. Developmental neuronal death in hippocampus requires the microglial CD11b integrin and DAP12 immunoreceptor. J. Neurosci. 28, 8138–8143.
Wang, I.T., et al., 2012. Loss of CDKL5 disrupts kinome profile and event-related potentials leading to autistic-like phenotypes in mice. Proc. Natl. Acad. Sci. U. S. A. 109, 21516–21521.
Watson, R.E., et al., 2006. Postnatal growth and morphological development of the brain: a species comparison. Birth Defects Res. B Dev. Reprod. Toxicol. 77, 471–484.
Wojcik, S.M., et al., 2004. An essential role for vesicular glutamate transporter 1 (VGLUT1) in postnatal development and control of quantal size. Proc. Natl. Acad. Sci. U. S. A. 101, 7158–7163.
Yuste, R., Bonhoeffer, T., 2004. Genesis of dendritic spines: insights from ultrastructural and imaging studies. Nat. Rev. Neurosci. 5, 24–34.
Zeiss, C.J., 2021. Comparative milestones in rodent and human postnatal central nervous system development. Toxicol. Pathol. 49, 1368–1373.
Zhu, Y.C., et al., 2013. Palmitoylation-dependent CDKL5-PSD-95 interaction regulates synaptic targeting of CDKL5 and dendritic spine development. Proc. Natl. Acad. Sci. U. S. A. 110, 9118–9123.